ChemEurJ

Research Article
doi.org/10.1002/chem.202502673

Chemistry Europe
European Chemical Societies Publishing

www.chemeurj.org

Substituent Effects on Sulfur Phenolate Exchange Reactions: Reactivity and Bonding Analysis

Akash Krishna,[a, b, c] Pau Besalú-Sala,[d] F. Matthias Bickelhaupt,[d, e, f] Guanna Li,*[c] and Han Zuilhof*[a, b]

The Sulfur Phenolate Exchange reaction (SuPhenEx) provides a fluorine-free alternative S(VI) exchange chemistry by substituting nitrophenolate as the leaving group instead of fluoride (as in SuFEx reactions), offering a synthetically appealing and environmentally friendly approach in click chemistry. Despite its significance, the reaction mechanism and the underlying electronic interactions in the course of the reaction have yet to be thoroughly explored at the molecular level. Here, we elucidate the electronic interactions of a series of SuPhenEx model reactions between various *para*-substituted phenolates (*p*-R-Ph-O^-) as nucleophiles and $PhSO_2$-OPh–*p*-NO_2 as an electrophile, in both gas and solvent (acetonitrile) phases. As tools, we apply the Activation Strain Model based on density functional theory. We identified the HOMO–LUMO interaction as the key determinant of reactivity in the gas phase, which shifts to include (HOMO-1)–(LUMO + 1) contributions in the solvent phase, and showed how these interactions can be tuned through the choice of the substituent in the *para*-substituted phenolate nucleophiles. The resulting insights, consistent across both phases, facilitate steering future experiments in these and related S(VI) substitution reactions.

1. Introduction

"Click chemistry," first coined by Sharpless et al., is a fruitful approach to emulate nature's preferred methods of synthesis for the fabrication of complex molecules.[1,2] This approach has become an increasingly important toolbox for constructing complex compounds and materials with high molecular diversity and tailored functionalities.[3–5] Click reactions are known for their modularity, broad applicability, stereospecificity, and atom economy, which enables high product yields. Increasingly, such reactions are also shown to be amenable to solvent-free, mechanochemical reaction conditions.[6,7] A few well-established examples of click reactions include the Cu(I)-catalyzed azide-alkyne cycloaddition (CuAAC),[8] analogous strain-promoted cycloadditions,[9–11] inverse electron-demand Diels-Alder reactions,[12] thiol C—C bond additions and, more recently, S(VI) exchange chemistries, such as the sulfur fluoride exchange (SuFEx) and sulfur phenolate exchange (SuPhenEx) reactions, which proceed via a bimolecular nucleophilic substitution at an electrophilic sulfur center (S_N2@S, see Scheme 1).[13]

SuFEx reactions have proven their biocompatibility, as demonstrated by the use of thionyl tetrafluoride (SOF_4)-derived connective hubs for efficient bioconjugation to DNA and proteins, while also showing promising applications in protein engineering, thus broadening the scope of bioorthogonal chemistry,[14–17] medicinal chemistry, and polymer chemistry.[18–23]

In this framework, our team developed the first enantiospecific click reaction via the SuFEx reaction of chiral sulfonimidoyl fluoride. Such asymmetric sulfur(VI)-centered chemistries have recently yielded significant attention, also given the rapid increase in SuFEx platforms.[24–26]

Furthermore, we expanded the scope of S(VI) exchange chemistry by using phenols with electron-withdrawing groups as leaving groups (such as *p*-NO_2-phenolate), as this strongly simplifies asymmetric syntheses (any of the two S(VI) enantiomers can now be made from one starting S(VI)-F or S(VI)-Cl compound), and allowed the introduction of the first dynamic covalent S(VI) click chemistry.[27] The so-called SuPhenEx reaction is fluorine-free and can proceed

[a] A. Krishna, H. Zuilhof
College of Biological and Chemical Engineering, Jiaxing University, Jiaxing 314001, China
E-mail: han.zuilhof@wur.nl

[b] A. Krishna, H. Zuilhof
Laboratory of Organic Chemistry, Wageningen University, Stippeneng 4, 6708 WE Wageningen, The Netherlands

[c] A. Krishna, G. Li
Biobased Chemistry and Technology, Wageningen University, Bornse Weilanden 9, 6708 WG Wageningen, The Netherlands
E-mail: Guanna.Li@WUR.nl

[d] P. Besalú-Sala, F. M. Bickelhaupt
Department of Chemistry and Pharmaceutical Sciences, AIMMS, Vrije Universiteit Amsterdam, 1081 HZ Amsterdam, The Netherlands

[e] F. M. Bickelhaupt
Institute for Molecules and Materials, Radboud University, Heyendaalseweg 135, 6525 AJ Nijmegen, The Netherlands

[f] F. M. Bickelhaupt
Department of Chemical Sciences, University of Johannesburg, Auckland Park, Johannesburg 2006, South Africa

Supporting information for this article is available on the WWW under https://doi.org/10.1002/chem.202502673

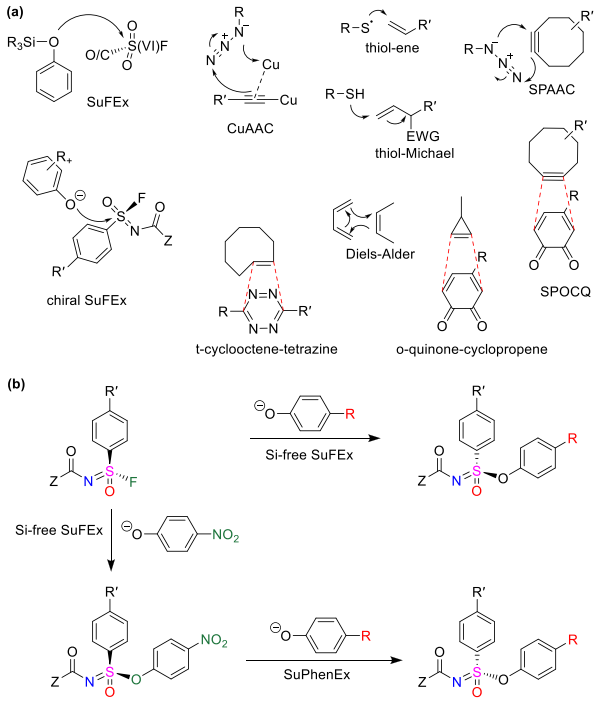

Scheme 1. (a) Selected click reactions. (b) SuFEx and SuPhenEx $S_N2@S$ reactions as asymmetric and dynamic covalent click chemistries.

enantiospecifically and quantitatively within 30 min at room temperature.[28,29]

In addition, it has recently been shown to be superior over SuFEx reactions in the synthesis of extended sequence-defined sulfonimidate oligomers.[30,31] Previously, the reaction mechanisms of the Si-free SuFEx and $Ca(NTf_2)_2$-mediated SuFEx were computationally predicted to follow either a concerted $S_N2@S$ process or an addition-elimination mechanism[32–37] with a short-lived intermediate, albeit that the stability of the intermediate is sometimes calculated within a kcal mol^{-1} of the TS and thereby lacks much experimental relevance for reactions at room temperature in a solvent. Conversely, the SuPhenEx reactions with phenolate anions across a broad range of substituents consistently indicated an $S_N2@S$ pathway.[27] In addition, recent detailed temperature-dependent kinetic studies of multimodal SuFEx and SuPhenEx click chemistries have highlighted the importance of both activation enthalpy ($\Delta H^{\ddagger}$) and activation entropy ($\Delta S^{\ddagger}$) in governing the reactivity.[38] The present computational study evaluates both, and then focuses on developing an understanding of the enthalpic barriers via energy decomposition analysis, while acknowledging entropy as a secondary but relevant factor for a more complete reactivity profile. In particular, the factors contributing to the high reaction rates, even at small driving forces, are not fully understood, nor is it clear how to enhance the reactivity of any S(VI) processes that would still require external conditions, such as heating or light irradiation[39] to proceed, particularly in applications like S(VI) exchange-based polymerization.[27]

In the current paper, we therefore aim to provide detailed insights into the enthalpic contributions to the activation barrier by focusing in-depth on the electronics of these S(VI)

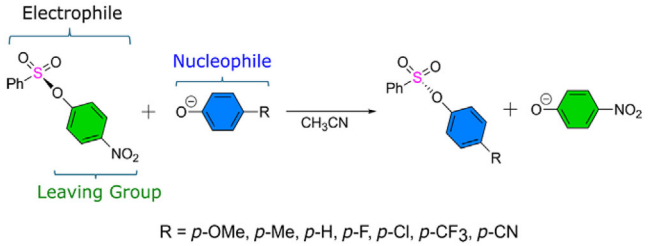

Scheme 2. General SuPhenEx reaction indicating the electrophile, nucleophile, and the leaving group.

exchange reactions. For this, we use quantum chemical simulations combined with comprehensive electronic property analysis for a prototype SuPhenEx reaction system, i.e., $PhSO_2OPh$-*p*-NO_2 as electrophile and a series of *para*-substituted phenolates as nucleophiles, i.e., methoxy (*p*-OMe), methyl (*p*-Me), hydrogen (*p*-H), fluorine (*p*-F), chlorine (*p*-Cl), trifluoromethyl (*p*-CF_3), and cyano (*p*-CN) (see Scheme 2). Specifically, we focus on three aspects: 1) what is the reaction mechanism, and what are the enthalpic effects of electronic substituents (electron-donating or electron-withdrawing) on the reaction rates? 2) what are the key electronic features contributing to the reactivity, as investigated by energy decomposition analysis? and 3) how do these observed factors compare in the gas and solvent phases (acetonitrile)?

2. Methods

Density functional theory (DFT) calculations were performed to obtain the activation barriers and reaction energies using Gaussian16.[40] The long-range-corrected ωB97XD functional,[41] including empirical dispersion combined with the triple-ζ 6–311+G(d,p) basis set,[42,43] was used in this study, as prior studies demonstrated that this combination produced results closely aligned with experimental results.[27,37] An SMD implicit solvation method was used to simulate the solvent effects of acetonitrile.[44] A benchmark study was performed for three solvation models to obtain a good tradeoff between reliability and model complexity, i.e., a continuum solvent model without Na^+ cation, a hybrid continuum-explicit solvent model, and a continuum solvent model with Na^+ cation.

To better understand the reactivity's underlying physical origins, we used the Activation Strain Model (ASM)[45–47] in combination with quantitative MO theory and a matching canonical energy decomposition analysis (EDA) as implemented in the Amsterdam Density Functional (ADF) program.[48] For such analyses of the electronic factors, we performed DFT computations with a method rather similar to ωB97XD/6–311+G(d,p) (which is not available in ADF), namely ωB97X/TZ2P, in both the gas phase and the solvent phase (acetonitrile, using the SMD12 solvation model), with the aim to explain the substituent effects of a strong electron-donating substituent (*p*-OMe) and those of a strong electron-withdrawing substituent (*p*-CN) on the barrier energies. An activation strain analysis relates the relative total energy of a molecular system during a chemical transformation

to the sum of the energies required to distort the separate reactants into the geometries that each of these has in the transition state (ΔE_{strain}) – that is, we distort the geometries, of the reactants, but keep them apart – plus the strength of the mutual interactions of such distorted geometries (ΔE_{int}). Then, the geometries along the reaction coordinate (ξ) are obtained via an IRC calculation, and at each point, the strain and interaction energy are obtained, see Eqn. (1). Here, $PhSO_2O(Ph\text{-}p\text{-}NO_2)$ (electrophile) is reactant A, and the phenolate (nucleophile) is reactant B.

$$\Delta E(\xi) = \Delta E_{strain}(\xi) + \Delta E_{int}(\xi) \quad (1)$$

In addition, the inter-fragment interaction $\Delta E_{int}(\xi)$ was further analyzed along the reaction coordinate using quantitative MO theory in conjunction with the canonical EDA method.[49,50] In this EDA, ΔE_{int} is decomposed into three physically meaningful terms, as shown in Eqn. 2:

$$\Delta E_{int}(\xi) = \Delta V_{elstat}(\xi) + \Delta E_{Pauli}(\xi) + \Delta E_{oi}(\xi) \quad (2)$$

Herein, ΔV_{elstat} is the classical electrostatic interaction between the intrinsic charge distributions of the interacting reactants, typically resulting in attraction. ΔE_{Pauli} is the Pauli repulsion that electrons experience, arising from the antisymmetrization of the reactants' wavefunctions. This term is proportional to the square of the overlap between occupied orbitals on either reactant (more precisely, the overlap between same-spin orbitals). It is responsible for any steric repulsion. ΔE_{oi} corresponds to the orbital interactions, including donor-acceptor interactions such as covalent or charge-transfer bonding mechanisms between occupied orbitals on one reactant and unoccupied orbitals on the other. Additionally, ΔE_{oi} includes polarization effects, which involve mixing empty and occupied orbitals on one reactant due to the presence of the other reactant.

Each pair of an occupied orbital on one reactant and an unoccupied orbital on the other reactant generates a stabilizing contribution to the overall orbital interactions ΔE_{oi} that is approximately proportional to the square of the overlap between the interacting orbitals (S^2) and inversely proportional to the energy difference ($\Delta\varepsilon$) between them:

$$\Delta E_{oi} \propto S^2/\Delta\varepsilon \quad (3)$$

Thus, significantly stabilizing orbital interactions ΔE_{oi} arise in situations with a significant overlap (large S^2) and a small energy gap $\Delta\varepsilon$ (large $1/\Delta\varepsilon$) between the involved orbitals.

3. Results and Discussion

The reaction mechanism study focused on the most plausible mechanism proposed in the literature, which involves nucleophilic substitution at the sulfur atom.[37] To investigate this mechanism and the associated electronic effects, we performed DFT computations in both gas and solvent phases, with the details of model construction, including the comparison of different solvent models, provided in the Supporting Information (Figure S1, Table S1).[21]

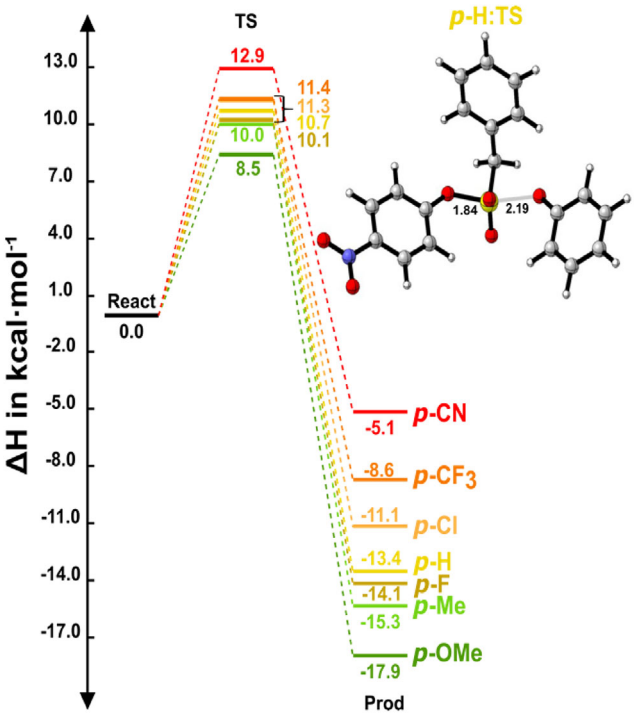

Figure 1. Reaction energy profile with nucleophiles ranging from EDG to EWG attacking $PhSO_2OPh\text{-}NO_2$ (electrophile), computed at SMD-ωB97XD/6–311+G(d,p).

The reaction complexes and transition states were optimized for the SuPhenEx reaction using phenolates with different substituents ranging from electron-donating groups (EDG) to electron-withdrawing groups (EWG), i.e., *p*-OMe, *p*-Me, *p*-H to *p*-F, *p*-Cl, *p*-CF_3, and *p*-CN, with Hammett substituent constants (σ_p) ranging from −0.27 to +0.66.[51] The resulting reaction energetics are presented in Figure 1. In all cases, only one transition state could be located, just like in the case of the SuPhenEx reaction with sulfonimidoyl derivatives,[27] meaning that all reactions follow a typical S_N2 mechanism, with the nucleophile approaching the electrophilic center from the backside (linear pathway). This aligns with earlier quantum chemical studies on S_N2 reactions at phosphorous(V) and other electrophilic centers, showing that unimodal S_N2 reaction profiles arise in solution and/or if substituents have sufficient steric demand.[52–55]

As the nucleophilicity decreases, the activation barriers increase, with the *p*-OMe phenolate exhibiting the lowest $\Delta H^{\ddagger}$ of 8.5 kcal mol^{-1} and the cyano-phenolate (*p*-CN) showing the highest $\Delta H^{\ddagger}$ of 12.9 kcal mol^{-1}. The same trend is followed for the reaction enthalpies where the reaction with the *p*-OMe- substituted phenolate is most feasible ($\Delta H = -17.9$ kcal mol^{-1}), going up to -5.1 kcal mol^{-1} for *p*-CN. The computed activation barriers aligned well with experimental reactivity trends observed at room temperature in previous studies: the *p*-OMe phenolate

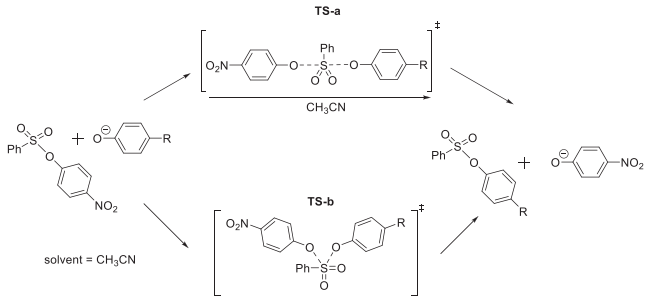

Scheme 3. Plausible reaction mechanisms: a) Linear one-step S_N2 mechanism, b) Side-on one-step S_N2 mechanism.

reacted in minutes, while the *p*-CN derivative took hours – both reactions, in fact, yielded a quantitative conversion.[28] While for the gas phase, taking *p*-OMe and *p*-CN as extreme cases for EDG and EWG, we found the same trend with *p*-OMe exhibiting a low $\Delta H^{\ddagger}$ of 6.2 kcal mol^{-1} and the *p*-CN showing the highest $\Delta H^{\ddagger}$ of 8.9 kcal mol^{-1}. But when comparing the gas phase and solvent phase reactions, clearly the gas phase displays an overall lower activation enthalpy barrier (Table S2). The inclusion of entropic effects further refines our understanding of SuPhenEx reactivity. The computed activation entropic penalty ($-T\Delta S^{\ddagger}$) of 1.0 to 2.5 kcal/mol on the free energy barrier ($\Delta G^{\ddagger}$ at 298.15 K) is consistent with an increased ordering in the transition state (Table S3). Compared to the computed $\Delta H^{\ddagger}$ values of 8.5 – 12.9 kcal/mol, this inclusion modestly raises $\Delta G^{\ddagger}$ without significantly affecting the overall ordering of substituent effects, and displays that – within the limits of the theoretical models used here — the enthalpic contribution is dominant.[38]

We also considered another viable reaction pathway where phenolate nucleophile attacks the $PhSO_2OPh\text{-}NO_2$ from the front side (side-on pathway, Scheme 3). However, the $\Delta H^{\ddagger}$ for the *p*-H phenolate via this pathway is significantly higher at 25.7 kcal mol^{-1}, compared to the 10.7 kcal mol^{-1} for the back-side attack (linear pathway). This difference arises from the steric hindrance between the phenyl rings of the phenolate nucleophile and the nitrophenolate leaving group, which obstructs the reaction in the higher-energy side-on pathway, and because of less favorable overlap between the lone-pair-type HOMO of the nucleophile and the substrate S—O σ^* antibonding acceptor orbital, as has been shown for various generic model systems.[56,57] For this reason, this side-on mechanism was disregarded.

Our results confirm that the $p\text{-}NO_2\text{-}Ph\text{-}O^-$ is a highly efficient leaving group. The reaction enthalpies are more negative than −5 kcal mol^{-1}, even for nucleophiles with strongly electron-withdrawing groups (EWGs), such as $p\text{-}CF_3$ and *p*-CN. This aligns with the experimental observations that reactions using these nucleophiles with EWGs can also provide a quantitative conversion under mild conditions.[28] Furthermore, we observed a linear correlation between the σ_p Hammett values and the calculated ratios for the rate constant $\log(k_x/k_H)$ (Figure S4). This set of reactions also holds good for a Bell-Evans-Polanyi (BEP) relationship, which states that the reaction energy is correlated with the activation barriers (Figure S4). Therefore, when knowing the experimental rates of a few substituents, σ_p or the overall reaction enthalpy/free energy can be used as descriptors to predict the activation barriers of other substituents, saving computing time spent on transition state calculations.

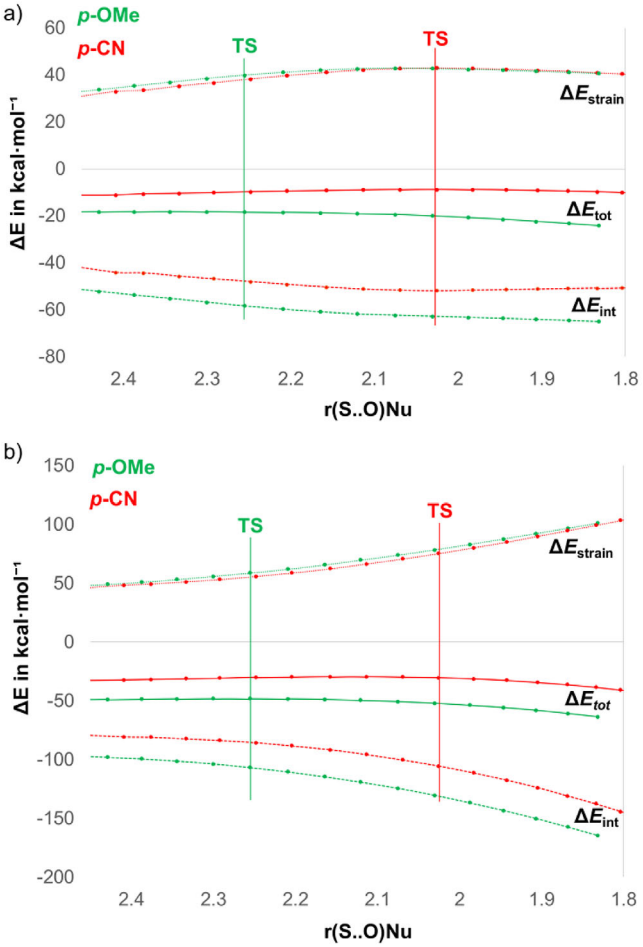

Figure 2. Activation strain analysis of p-OMe (green) and p-CN (red) phenolate reacting with the $PhSO_2O(Ph\text{-}p\text{-}NO_2)$ substrate, computed at the SMD-ωB97X/TZ2P level of theory: (a) gas phase, (b) solvent phase (acetonitrile). Notes: Green vertical line = location TS of p-OMe; red vertical line = location TS of p-CN. r(S–O)_Nu = distance between nucleophile and sulfur atom.

Next, analyses based on the ASM and quantitative MO theory were performed to better understand the intrinsic factors influencing the reactivity of this set of SuPhenEx reactions, taking *p*-OMe and *p*-CN representative cases for EDG and EWG, respectively. The activation strain diagram in Figure 2 illustrates the differences between the *p*-OMe and *p*-CN substituents in terms of ΔE_{strain}, ΔE_{tot}, and ΔE_{int}, along the reaction coordinate, defined by the $S\text{–}O_{(nucleophile)}$ bond distance r(S…O)Nu, in both gas phase (Figure 2a) and solvent phase (acetonitrile, Figure 2b). In the gas phase, along the entire reaction coordinate, *p*-OMe exhibits a more stabilizing nucleophile–substrate interaction curve ΔE_{int} than *p*-CN. The strain curves are nearly identical for both *p*-OMe and *p*-CN. The similarity in the strain curves results from the fact that the main contributor of strain in the reactants is the breaking of the $S\text{–}O_{(leaving\ group)}$ bond, which is indeed identical in both reactions. Thus, the acceleration of the reaction for *p*-OMe compared to *p*-CN is due to the more

favorable orbital interactions; we address the reason for this later on. The fact that *p*-OMe has a lower barrier than *p*-CN nicely agrees with previous experimental and computational reports on the SuPhenEx reaction in sulfonimidoyl analogs.[27] In the solvent phase, we observe the same trends, although the overall stabilization is enhanced in the solvent compared to the gas phase

Note that the TS of the *p*-OMe at r(S–O)Nu = 2.26 Å occurs earlier along the reaction coordinate than that of the *p*-CN at r(S–O)Nu = 2.03 Å. This Hammond behavior is related to the more stabilizing and, therefore, also slightly steeper ΔE_{int} curve for *p*-OMe, which, for two essentially equal ΔE_{strain} curves, pulls the maximum of $\Delta E(\xi) = \Delta E_{strain}(\xi) + \Delta E_{int}(\xi)$ to an earlier point along the reaction coordinate ξ.

Now, we return to why the interaction ΔE_{int} with the $PhSO_2OPh\text{-}NO_2$ substrate is more stabilizing for the *p*-OMe than the *p*-CN nucleophile. The energy decomposition analysis (EDA) of ΔE_{int} along the reaction coordinate (Figure 3) shows that, in the gas phase (Figure 3a), the orbital interactions ΔE_{oi} are clearly more favorable for the *p*-OMe than the *p*-CN reaction. In contrast, ΔV_{elstat} and ΔE_{Pauli} are very similar for both; the last one being evident to organic chemists from another point of view: the difference in steric interactions for these *para*-substituted nucleophiles will be minimal. Therefore, the orbital interactions determine the preference for the reaction with *p*-OMe over that with *p*-CN.

In the solvent phase (acetonitrile, Figure 3b), the EDA reveals a shift in the contributions to ΔE_{int}. The orbital interactions ΔE_{oi} become less favorable for both p-OMe and p-CN compared to the gas phase. However, ΔV_{elstat} becomes significantly more stabilizing in the solvent, dominating the interaction energy and driving the more negative ΔE_{int} for both nucleophiles, with p-OMe still benefiting more than *p*-CN. The ΔE_{Pauli} term remains similar for both nucleophiles and is comparable to the gas phase. An enlarged view (Figure 3c) of the solvent phase curves highlights that the ΔE_{oi} of p-OMe remains slightly more favorable than that of *p*-CN, while the larger difference in ΔV_{elstat} further favors *p*-OMe. Compared to the sulfonimidoyl system reported previously,[27] which showed distortion-controlled reactivity due to the presence of bulky phenyl groups @S, the current sulfonyl substrate is both less sterically hindered and more electrophilic. As a result, the variation in distortion energy along the IRC is smaller, and reactivity is mainly governed by ΔE_{oi} in the gas phase, and by a combination of ΔV_{elstat} and ΔE_{oi} in the solvent phase. This reflects a shift from distortion control to interaction control caused by the change in the nature of the sulfur electrophile. These results underscore the role of solvent polarity in modulating reactivity mechanisms, shifting emphasis from orbital to electrostatic control in going from apolar to polar solvents, particularly for polarizable electrophiles like sulfonyl derivatives. This insight provides a conceptual basis for tuning reaction barriers through solvent screening, offering a valuable strategy for rational reaction design.

To get a more in-depth understanding of this orbital interaction effect, we performed a Kohn-Sham molecular orbital (KS-MO) analysis of ΔE_{oi} where the bond length of the bond between (electrophile) S…O (nucleophile) is ~2.15 Å (Figure 4),

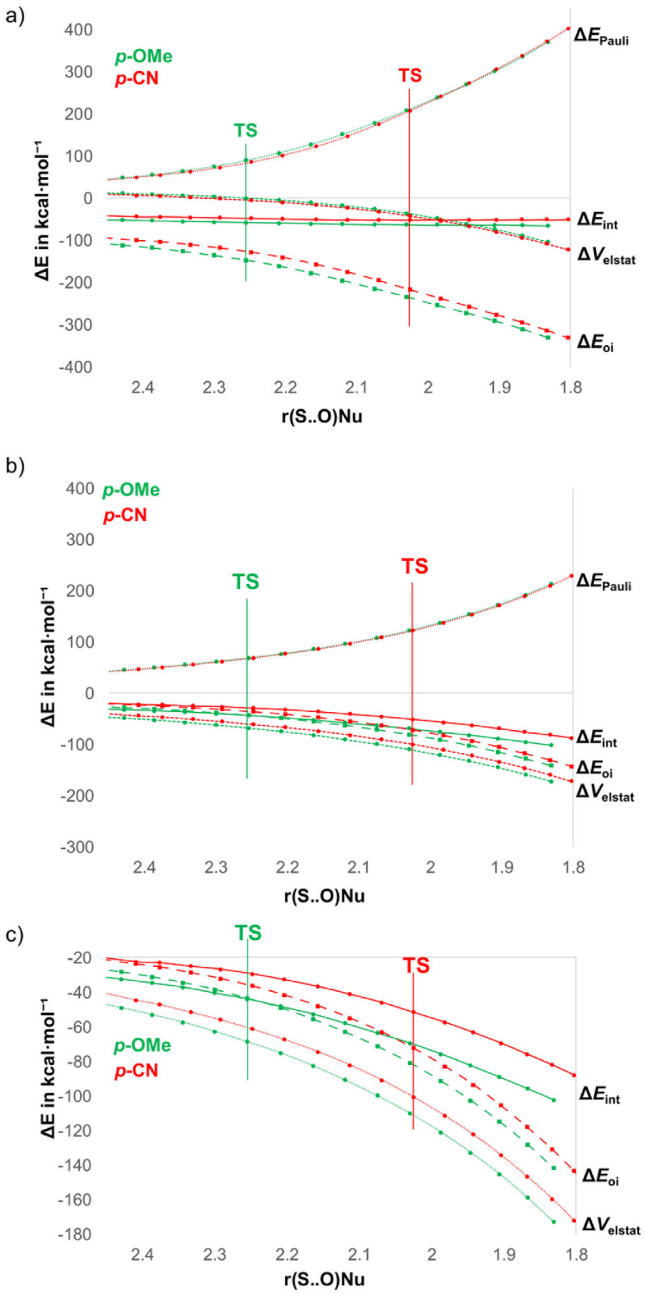

Figure 3. Energy decomposition analysis of p-OMe (green) and p-CN (red) computed at SMD-ωB97X/TZ2P: (a) gas phase, (b) solvent phase (acetonitrile), and (c) enlarged view of solvent phase curves. Green vertical line = location TS of p-OMe; red vertical line = location TS of p-CN. r(S–O)Nu = distance between the nucleophile and the sulfur atom.

which is approximately a point in the middle between the TSs of *p*-OMe (green) and *p*-CN (red). Additionally, calculations performed at another point (~2.07 Å) along the reaction coordinate bear the same conclusions for the gas phase, demonstrating that the results are consistent regardless of the position along the reaction path (Figure S5).[58]

To simplify the representation of the orbitals involved, only the primary interactions between the frontier orbitals, including $(HOMO\text{-}1)_{Nu}$, $HOMO_{Nu}$, $LUMO_{Elec}$ and $(LUMO + 1)_{Elec}$ in the gas phase, are highlighted in Figure 4. Specifically, we show

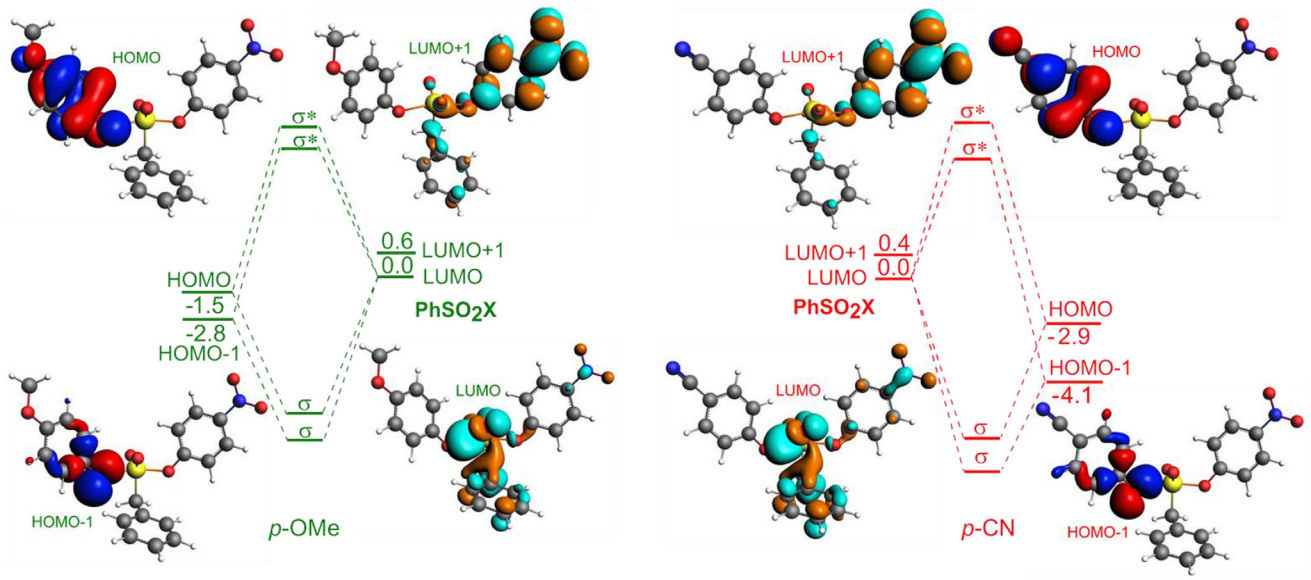

Figure 4. Orbital interaction diagram for HOMO-LUMO and HOMO-1-LUMO interaction in the SuPhenEx reactions with p-OMe-phenolate and p-CN-phenolate with **1** upon formation of S. .O(Nu) bond at a distance of ~2.15 Å computed at ωB97X/TZ2P calculations in the gas phase and the energies are in eV. Here LUMO and LUMO + 1 are of $PhSO_2X$ substrate, and HOMO and HOMO-1 are of the phenolates, i.e., p-OMe (green) and p-CN (red).

Table 1. Orbital overlap (*S*) and energy gap ($\Delta\varepsilon$) of *p*-OMe and *p*-CN computed at ωB97X/TZ2P in the gas phase. Here, $LUMO_{Elec}$ is of $PhSO_2X$ substrate, and $HOMO_{Nu}$ and $HOMO^{-1}{}_{Nu}$ are of the phenolates (*p*-OMe and *p*-CN).

Nucleophile	Interactions	*S*	$\Delta\varepsilon$ (eV)	$S^2/\Delta\varepsilon$
***p*-OMe**	$HOMO_{Nu}$-$LUMO_{Elec}$	0.003	1.5	6.31E-02
	$HOMO_{Nu}$-LUMO + 1_{Elec}	0.006	2.2	4.36E-04
	$HOMO\text{-}1_{Nu}$-$LUMO_{Elec}$	0.010	2.8	1.08E-01
	$HOMO\text{-}1_{Nu}$-LUMO + 1_{Elec}	0.016	3.4	2.57E-03
***p*-CN**	$HOMO_{Nu}$-$LUMO_{Elec}$	0.025	3.0	5.79E-03
	$HOMO_{Nu}$-LUMO + 1_{Elec}	0.005	3.3	7.69E-05
	$HOMO\text{-}1_{Nu}$-$LUMO_{Elec}$	0.118	4.1	9.33E-05
	$HOMO\text{-}1_{Nu}$-LUMO + 1_{Elec}	0.033	4.5	1.75E-03

that the HOMO of the nucleophile ($HOMO_{Nu}$), located at the oxygen, interacts with the $PhSO_2OPh\text{-}NO_2$ orbital ($LUMO_{Elec}$). KS-MO analysis reveals that the $HOMO_{Nu}$–$LUMO_{Elec}$ interaction is stronger for nucleophiles with *p*-OMe substituents compared to those with *p*-CN substituents (Figure 4). The strength of this interaction is reflected in the orbital overlap (S), which is significantly larger for *p*-OMe ($S = 0.059$) than for *p*-CN ($S = 0.025$) (Table 1). Additionally, the energy gap ($\Delta\varepsilon$) between $HOMO_{Nu}$-$LUMO_{Elec}$ is smaller for *p*-OMe ($\Delta\varepsilon = 1.5$ eV) than for p-CN ($\Delta\varepsilon = 2.9$ eV), further favoring stronger interaction. Therefore, the ratio $S^2/\Delta\varepsilon$ reflects this, with values of 6.30E-02 for *p*-OMe and 6.00E-03 for *p*-CN, confirming the stronger $HOMO_{Nu}$-$LUMO_{Elec}$ interaction for *p*-OMe. Although $S(HOMO\text{-}1_{Nu}/LUMO_{Elec})$ increases from 0.105 for *p*-OMe to 0.118 for *p*-CN (a relative increase of 27%, favoring *p*-CN), the energy gap for these orbitals increases more dramatically, from 2.8 eV (*p*-OMe) to 4.1 eV (*p*-CN), a 50% relative increase that favors *p*-OMe. This larger gap difference compared to the change in orbital overlap *S* is the key reason for the more stabilizing $(HOMO\text{-}1)_{Nu}$-$LUMO_{Elec}$ interaction in *p*-OMe systems. While the $(LUMO + 1)_{Elec}$ is not particularly high in energy, its interactions with the HOMO and HOMO-1 of the nucleophile are much weaker than those involving the LUMO, and thus do not significantly influence the reaction energetics. Thus, both $(HOMO\text{-}1)_{Nu}$-$LUMO_{Elec}$ and $HOMO_{Nu}$-$LUMO_{Elec}$ interactions are more favorable for the *p*-OMe over the *p*-CN, adding up to a more stabilizing ΔE_{oi} for the *p*-OMe, a determining effect that lowers its activation barrier.

In the solvent phase (acetonitrile, Figure 5), the KS-MO analysis at the same point (~2.15 Å) shows that the $(LUMO + 1)_{Elec}$ becomes relevant, unlike in the gas phase, due to the solvent's stabilization of the orbitals of the nucleophile. The primary interactions still involve $HOMO_{Nu}$ and $(HOMO\text{-}1)_{Nu}$ but now include $(LUMO + 1)_{Elec}$ alongside $LUMO_{Elec}$. The $HOMO_{Nu}$–$LUMO_{Elec}$ interaction weakens for both nucleophiles due to the larger energy gap ($\Delta\varepsilon$), which increases to 6.39 eV for p-OMe and 7.15 eV for *p*-CN, compared to 1.5 eV and 2.9 eV in the gas phase, respectively. The orbital overlap *S* also decreases, with values of 0.026 for *p*-OMe and −0.007 for *p*-CN (Table 2), reflecting the reduced interaction strength. Consequently, the ratio $S^2/\Delta\varepsilon$ drops significantly to 1.04E-04 for *p*-OMe and 6.76E-06 for *p*-CN, confirming the weaker $HOMO_{Nu}$–$LUMO_{Elec}$ interaction in the solvent phase. The $(HOMO\text{-}1)_{Nu}$–$LUMO_{Elec}$ interaction also weakens, with $\Delta\varepsilon$ increasing to 8.04 eV for *p*-OMe and 8.52 eV for *p*-CN, and *S* values of −0.046 for *p*-OMe.

Comparing the gas and solvent phases, the gas phase shows stronger $HOMO_{Nu}$–$LUMO_{Elec}$ and $(HOMO\text{-}1)_{Nu}$–$LUMO_{Elec}$ interactions for *p*-OMe, driven by smaller energy gaps and larger overlaps, leading to a more stabilizing ΔE_{oi} and a lower barrier. In the solvent phase, the increased $\Delta\varepsilon$ weakens these interactions for both nucleophiles. Still, *p*-OMe maintains an overall more stabilizing ΔE_{oi} in most interactions, particularly $HOMO_{Nu}$–$LUMO_{Elec}$, $HOMO_{Nu}$–$(LUMO + 1)_{Elec}$, and $(HOMO\text{-}1)_{Nu}$–$LUMO_{Elec}$,

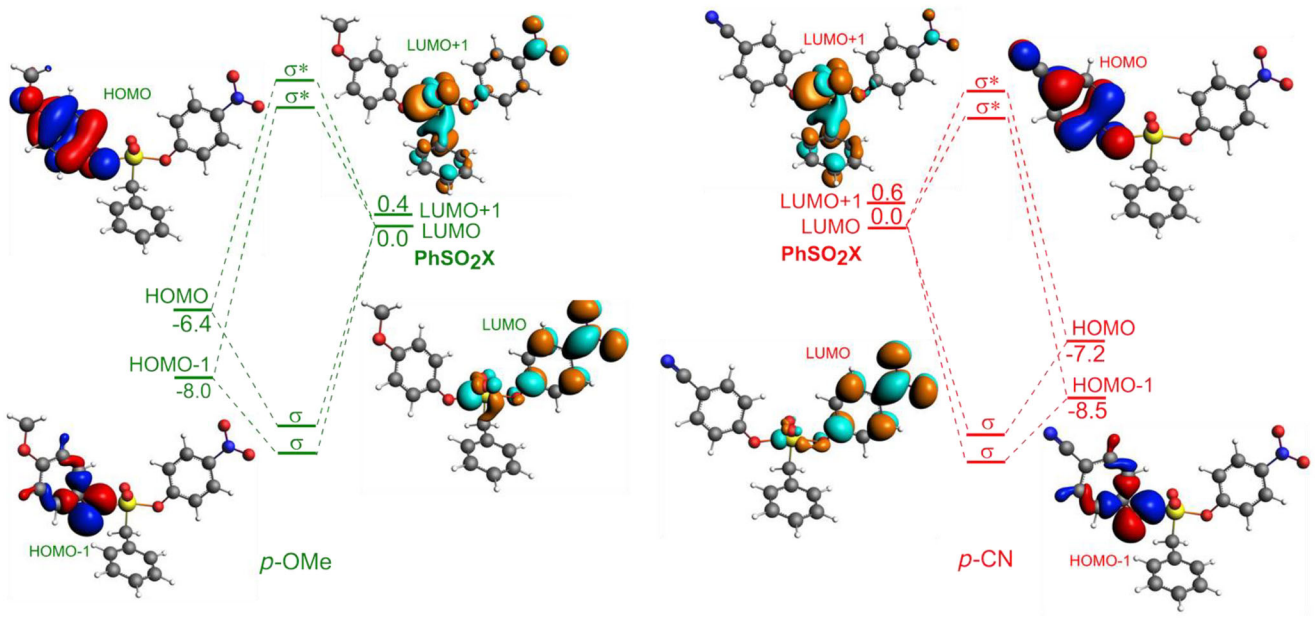

Figure 5. Orbital interaction diagram for HOMO-LUMO and HOMO-1-LUMO interaction in the SuPhenEx reactions with p-OMe-phenolate and p-CN-phenolate with **1** upon formation of S. .O(Nu) bond at a distance of ~2.15 Å (ωB97X/TZ2P calculations in solvent phase (acetonitrile); energies in eV). Here LUMO and LUMO + 1 are of $PhSO_2X$ substrate, and HOMO and HOMO-1 are of the phenolates, i.e., p-OMe (green) and p-CN (red).

Table 2. Orbital overlap (S), and energy gap ($\Delta\varepsilon$) of p-OMe and p-CN computed at ωB97X/TZ2P in the solvent phase. Here, $LUMO_{Elec}$ and $LUMO + 1_{Elec}$ are of $PhSO_2X$ substrate, and $HOMO_{Nu}$ and $HOMO^{-1}{}_{Nu}$ are of the phenolates (p-OMe and p-CN).

Nucleophile	Interactions	S	$\Delta\varepsilon$ (eV)	$S^2/\Delta\varepsilon$
***p*-OMe**	$HOMO_{Nu}$-$LUMO_{Elec}$	0.026	6.4	1.04E-04
	$HOMO_{Nu}$-$LUMO + 1_{Elec}$	−0.050	6.8	3.72E-04
	$HOMO\text{-}1_{Nu}$-$LUMO_{Elec}$	−0.046	8.0	2.63E-04
	$HOMO\text{-}1_{Nu}$-$LUMO + 1_{Elec}$	0.102	8.5	1.23E-03
***p*-CN**	$HOMO_{Nu}$-$LUMO_{Elec}$	−0.007	7.2	6.76E-06
	$HOMO_{Nu}$-$LUMO + 1_{Elec}$	0.024	7.8	7.69E-05
	$HOMO\text{-}1_{Nu}$-$LUMO_{Elec}$	0.028	8.5	9.33E-05
	$HOMO\text{-}1_{Nu}$-$LUMO + 1_{Elec}$	−0.126	9.1	1.75E-03

due to consistently smaller energy gaps and more favorable $S^2/\Delta\varepsilon$ values, except for the $(HOMO\text{-}1)_{Nu}$–$(LUMO + 1)_{Elec}$ interaction, where *p*-CN gains an advantage. However, the solvent phase's enhanced electrostatic effects (Figure 3b–c) complement the orbital interactions, a determining effect that lowers the activation barrier of *p*-OMe.

Two key factors govern the nucleophilicity in these SuPhenEx reactions: the $HOMO_{Nu}$–$LUMO_{Elec}$ gap ($\Delta\varepsilon$), which reflects the stability of the $HOMO_{Nu}$ relative to the $LUMO_{Elec}$, and the orbital population. However, the impact of orbital population differences on nucleophilicity is negligible in both gas and solvent phases, and the primary determining factor remains the $HOMO_{Nu}$–$LUMO_{Elec}$ gap ($\Delta\varepsilon$) in the gas phase, where *p*-OMe exhibits a smaller gap (1.50 eV) compared to *p*-CN (2.90 eV). In the solvent phase (acetonitrile), the $HOMO_{Nu}$–$LUMO_{Elec}$ gap increases (6.39 eV for *p*-OMe, 7.15 eV for *p*-CN), but p-OMe still maintains a smaller gap, reinforcing its greater nucleophilicity, with additional contributions from the $(HOMO\text{-}1)_{Nu}$–$(LUMO + 1)_{Elec}$ interaction. More details, including orbital population data, are provided in the Supporting Information (Table S4-S5).

These findings align with the established principle that electron-donating substituents like *p*-OMe push the occupied orbitals to higher energy levels ($HOMO_{Nu}$ at -6.39 eV in solvent). In comparison, electron-withdrawing groups like *p*-CN lower the energy of these orbitals ($HOMO_{Nu}$ at -7.15 eV in solvent). While the LUMO of the electrophile may also contribute to the energy gap, in this case, its variation between *p*-OMe and *p*-CN substituents is minimal, as the electrophile ($PhSO_2OPh\text{-}NO_2$) is identical in both reactions. Thus, the primary effect arises from *p*-OMe and *p*-CN pushing their respective occupied orbitals up and down in energy. These combined effects result in stronger orbital interactions for *p*-OMe, which become more significant as the electron-donating strength increases. This trend holds in both gas and solvent phases but is amplified in the latter due to the enhanced energy gap.

4. Conclusions

Sulfur Phenolate Exchange Reactions (SuPhenEx) proceed via a single-step, linear $S_N2@S$ mechanism. Detailed Activation Strain and quantitative MO analyses reveal for model SuPhenEx reactions of $R\text{-}Ph\text{-}O^- + PhSO_2OPh\text{-}p\text{-}NO_2$ (R = *p*-MeO or *p*-CN), conducted in the gas phase and solvent phase (acetonitrile), that a more electron-donating substituent makes the *para*-substituted phenolate a better nucleophile by pushing its oxygen lone-pair-type HOMO up in energy. This reduces the corresponding $HOMO_{Nu}$–$LUMO_{Elec}$ gap with the S–O σ*-type $LUMO_{Elec}$ of the

$PhSO_2OPh$-p-NO_2 substrate in such $S_N2@S$ substitutions, and thus strengthens the $HOMO_{Nu}$–$LUMO_{Elec}$ orbital interactions. In the gas phase, this effect directly stabilizes the nucleophile–substrate interaction and lowers the enthalpic reaction barrier. In contrast, in the solvent phase, the $HOMO_{Nu}$–$LUMO_{Elec}$ gap increases due to the solvent's stabilization of the nucleophile's HOMO, thereby weakening the orbital interactions, but the enhanced electrostatic interactions, as shown by a more stabilizing ΔV_{elstat}, further stabilize the nucleophile–substrate interaction, maintaining *p*-OMe's advantage as a stronger nucleophile. Consequently, the height of the reaction barrier remains lower for electron-donating substituents in both phases, with the solvent amplifying the energy gap effect while adding a cooperative electrostatic stabilization. This shows that both the reaction barrier and the enthalpic factors that constitute this can be tuned by choosing the appropriate solvent, which can help in reaction condition optimization.

These insights provide a comprehensive view on the enthalpic components of the reaction barrier, which can be leveraged to design nucleophiles, substrates, and catalysts that enhance and optimize the rate of the SuPhenEx reaction as an effective, fluorine-free variant of S(VI) exchange chemistries. While our analysis offers detailed insight into the enthalpic driving forces, it will be useful for future work needed to assess entropic and dynamic solvent contributions to S(VI) exchange reactivity.

Acknowledgments

The authors gratefully acknowledge the extensive support provided by a Top-Talent Grant of Zhejiang Province (Jiaxing University; to H.Z.), and Wageningen University. This research was part of the Sector Plan Engineering II, funded by the Dutch Ministry of Education, Culture, and Science (OCW). The simulations were conducted using the Dutch national e-infrastructure, with the support of the SURF Cooperative (EINF-8821, NWO-2025.019/L1), and the VU-Bazis computational resources.

Conflict of Interest

The authors declare no conflict of interest.

Data Availability Statement

Data sharing is not applicable to this article as no new data were created or analyzed in this study.

Supporting Information

The data that support the findings of this study are available in the supplementary material of this article.

Keywords: bonding analysis · click reactions · density functional theory calculations · sufex · suphenex

[1] H. C. Kolb, M. G. Finn, K. B. Sharpless, *Angew. Chem., Int. Ed.* **2001**, *40*, 2004. https://doi.org/10.1002/1521-3773(20010601)40:11⟨2004::AID-ANIE2004⟩3.0.CO;2-5.
[2] J. Escorihuela, A. T. M. Marcelis, H. Zuilhof, *Adv. Mater. Interfaces* **2015**, *2*, https://doi.org/10.1002/admi.201570063.
[3] H. C. Kolb, K. B. Sharpless, *Drug Discov Today* **2003**, *8*, 1128. https://doi.org/10.1016/S1359-6446(03)02933-7.
[4] B. Albada, J. F. Keijzer, H. Zuilhof, F. van Delft, *Chem. Rev.* **2021**, *121*, 7032. https://doi.org/10.1021/acs.chemrev.0c01180.
[5] K. Ghosal, S. K. Bhattacharyya, V. Mishra, H. Zuilhof, *Chem. Rev.* **2024**, *124*, 13216. https://doi.org/10.1021/acs.chemrev.4c00251.
[6] Y. Wang, Z. Hao, M. Islam, Y. Zhu, Y. Chao, S. P. Pujari, H. Zuilhof, *Adv. Synth. Catal.* **2025**, *n/a*, DOI https://doi.org/10.1002/adsc.202500254.
[7] S. Tripathi, S. P. Pujari, M. Romkes, F. M. Miloserdov, H. Zhou, H. Zuilhof, *ChemistryEurope* **2025**, *n/a*, 2500006.
[8] V. V. Rostovtsev, L. G. Green, V. V. Fokin, K. B. Sharpless, *Angew. Chem., Int. Ed.* **2002**, *41*, 2596. https://doi.org/10.1002/1521-3773(20020715)41:14⟨2596::AID-ANIE2596⟩3.0.CO;2-4.
[9] D. Gahtory, R. Sen, A. R. Kuzmyn, J. Escorihuela, H. Zuilhof, *Angew. Chem., Int. Ed.* **2018**, *57*, 10118. https://doi.org/10.1002/anie.201800937.
[10] N. J. Agard, J. A. Prescher, C. R. Bertozzi, *J. Am. Chem. Soc.* **2004**, *126*, 15046. https://doi.org/10.1021/ja044996f.
[11] A. Borrmann, O. Fatunsin, J. Dommerholt, A. M. Jonker, D. W. P. M. Löwik, J. C. M. van Hest, F. L. van Delft, *Bioconjug Chem* **2015**, *26*, 257. https://doi.org/10.1021/bc500534d.
[12] K. A. Jørgensen, *Angew. Chem.* **2000**, *39*, 3558. https://doi.org/10.1002/1521-3773(20001016)39:20⟨3558::AID-ANIE3558⟩3.0.CO;2-I.
[13] J. Dong, L. Krasnova, M. G. Finn, K. B. Sharpless, *Angew. Chem., Int. Ed.* **2014**, *53*, 9430. https://doi.org/10.1002/anie.201309399.
[14] S. Li, P. Wu, J. E. Moses, K. B. Sharpless, *Angew. Chem., Int. Ed.* **2017**, *56*, 2903. https://doi.org/10.1002/anie.201611048.
[15] Q. Zheng, J. L. Woehl, S. Kitamura, D. Santos-Martins, C. J. Smedley, G. Li, S. Forli, J. E. Moses, D. W. Wolan, K. B. Sharpless, *Proc. Natl. Acad. Sci. USA* **2019**, *116*, 18808. https://doi.org/10.1073/pnas.1909972116.
[16] A. Marra, C. Nativi, A. Dondoni, *New J. Chem.* **2020**, *44*, 4678. https://doi.org/10.1039/D0NJ00504E.
[17] F. Liu, H. Wang, S. Li, G. A. L. Bare, X. Chen, C. Wang, J. E. Moses, P. Wu, K. B. Sharpless, *Angew. Chem., Int. Ed.* **2019**, *58*, 8029. https://doi.org/10.1002/anie.201902489.
[18] C. J. Smedley, G. Li, A. S. Barrow, T. L. Gialelis, M.-C. Giel, A. Ottonello, Y. Cheng, S. Kitamura, D. W. Wolan, K. B. Sharpless, J. E. Moses, *Angew. Chem., Int. Ed.* **2020**, *59*, 12460. https://doi.org/10.1002/anie.202003219.
[19] A. S. Barrow, C. J. Smedley, Q. Zheng, S. Li, J. Dong, J. E. Moses, *Chem. Soc. Rev.* **2019**, *48*, 4731. https://doi.org/10.1039/C8CS00960K.
[20] M. P. Kim, S. Kayal, C. Hwang, J. Bae, H. Kim, D. G. Hwang, M. H. Jeon, J. K. Seo, D. Ahn, W. Lee, S. Seo, J.-H. Chun, Y. Yu, S. Y. Hong, *Nat. Commun.* **2024**, *15*, 3381. https://doi.org/10.1038/s41467-024-47567-z.
[21] M. Wang, J. Hou, H. Do, C. Wang, X. Zhang, Y. Du, Q. Dong, L. Wang, K. Ni, F. Ren, J. An, *Nat. Commun.* **2024**, *15*, 6849. https://doi.org/10.1038/s41467-024-50922-9.
[22] S. Zhao, D. Zeng, M. Wang, X. Jiang, *Nat. Commun.* **2024**, *15*, 727. https://doi.org/10.1038/s41467-024-44998-6.
[23] L. Xu, P. Wu, J. Dong in, *Synthetic Polymer Chemistry: Innovations and Outlook* (Eds.: Z. Zhao, R. Hu, A. Qin, B.Z. Tang), The Royal Society Of Chemistry, **2019**, pp. 1–31.
[24] Y. Chao, M. Subramaniam, K. Namitharan, Y. Zhu, V. Koolma, Z. Hao, S. Li, Y. Wang, I. Hudoynazarov, F. M. Miloserdov, H. Zuilhof, *J. Org. Chem.* **2023**, *88*, 15658. https://doi.org/10.1021/acs.joc.3c01656.
[25] N. Lional, F. M. Miloserdov, H. Zuilhof, *Angew. Chem., Int. Ed.* **2024**, *63*, e202406915. https://doi.org/10.1002/anie.202406915.
[26] D.-D. Liang, S. P. Pujari, M. Subramaniam, M. Besten, H. Zuilhof, *Angew. Chem., Int. Ed.* **2022**, *61*, e202116158. https://doi.org/10.1002/anie.202116158.
[27] Y. Chao, A. Krishna, M. Subramaniam, D. Liang, S. P. Pujari, A. C.-H. Sue, G. Li, F. M. Miloserdov, H. Zuilhof, *Angew. Chem., Int. Ed.* **2022**, 61, https://doi.org/10.1002/anie.202207456.
[28] A. F. J. van den Boom, M. Subramaniam, H. Zuilhof, *Org. Lett.* **2022**, *24*, 8621. https://doi.org/10.1021/acs.orglett.2c03421.

[29] A. F. J. van den Boom, H. Zuilhof, *Org. Lett.* **2023**, *25*, 788. https://doi.org/10.1021/acs.orglett.2c04292.
[30] Y. Han, D.-D. Liang, S. Heskamp, B. Chen, F. M. Miloserdov, H. Zuilhof, *ChemistryEurope* **2025**, *submitted* https://doi.org/10.1002/ceur.202500324.
[31] Y. Han, S. P. Pujari, M. Subramaniam, B. Chen, F. M. Miloserdov, H. Zuilhof, *Nature Synthesis* **2025**, https://doi.org/10.1038/s44160-025-00805-8.
[32] S. Mahapatra, C. P. Woroch, T. W. Butler, S. N. Carneiro, S. C. Kwan, S. R. Khasnavis, J. Gu, J. K. Dutra, B. C. Vetelino, J. Bellenger, C. W. am Ende, N. D. Ball, "SuFEx Activation with Ca(NTf2)2: A Unified Strategy to Access Sulfamides, Sulfamates, and Sulfonamides from S(VI) Fluorides" Org. Lett. **2020**, *22*, 4389. https://doi.org/10.1021/acs.orglett.0c01397.
[33] D.-D. Liang, N. Lional, B. Scheepmaker, M. Subramaniam, G. Li, F. M. Miloserdov, H. Zuilhof, *Org. Lett.* **2023**, *25*, 5666. https://doi.org/10.1021/acs.orglett.3c02132.
[34] S. Greed, O. Symes, J. A. Bull, *Chem. Commun.* **2022**, *58*, 5387. https://doi.org/10.1039/D2CC01219G.
[35] J.-N. Luy, R. Tonner, *ACS Omega* **2020**, *5*, 31432. https://doi.org/10.1021/acsomega.0c05049.
[36] B. Han, S. R. Khasnavis, M. Nwerem, M. Bertagna, N. D. Ball, O. M. Ogba, *Inorg. Chem.* **2022**, *61*, 9746. https://doi.org/10.1021/acs.inorgchem.2c01230.
[37] D.-D. Liang, D. E. Streefkerk, D. Jordaan, J. Wagemakers, J. Baggerman, H. Zuilhof, *Angew. Chem., Int. Ed.* **2020**, *59*, 7494. https://doi.org/10.1002/anie.201915519.
[38] Y. Zhu, A. Krishna, Y. Chao, X. Li, S. P. Pujari, G. Li, H. Huang, H. Zhao, J. Dong, H. Zuilhof, *J. Org. Chem.* **2025**, https://doi.org/10.1021/acs.joc.5c00615.
[39] S. T. Shreiber, G. A. Molander, *Org. Lett.* **2023**, *25*, 2084. https://doi.org/10.1021/acs.orglett.3c00447.
[40] M. J. Frisch, G. W. Trucks, H. B. Schlegel, G. E. Scuseria, M. A. Robb, J. R. Cheeseman, G. Scalmani, V. Barone, G. A. Petersson, H. Nakatsuji, X. Li, M. Caricato, A. V. Marenich, J. Bloino, B. G. Janesko, R. Gomperts, B. Mennucci, H. P. Hratchian, J. V. Ortiz, A. F. Izmaylov, J. L. Sonnenberg, F. D. Williams, F. Lipparini, F. Egidi, J. Goings, B. Peng, A. Petrone, T. Henderson, D. Ranasinghe, V. G. Zakrzewski, J. Gao, N. Rega, G. Zheng, W. Liang, M. Hada, M. Ehara, K. Toyota, R. Fukuda, J. Hasegawa, M. Ishida, T. Nakajima, Y. Honda, O. Kitao, H. Nakai, T. Vreven, K. Throssell, J. A. Montgomery Jr, J. E. Peralta, F. Ogliaro, M. J. Bearpark, J. J. Heyd, E. N. Brothers, K. N. Kudin, V. N. Staroverov, T. A. Keith, R. Kobayashi, J. Normand, K. Raghavachari, A. P. Rendell, J. C. Burant, S. S. Iyengar, J. Tomasi, M. Cossi, J. M. Millam, M. Klene, C. Adamo, R. Cammi, J. W. Ochterski, R. L. Martin, K. Morokuma, O. Farkas, J. B. Foresman, D. J. Fox, **2016**.
[41] N. Mardirossian, M. Head-Gordon, *Phys. Chem. Chem. Phys.* **2014**, *16*, 9904. https://doi.org/10.1039/c3cp54374a.
[42] A. D. McLean, G. S. Chandler, *J. Chem. Phys.* **1980**, *72*, 5639. https://doi.org/10.1063/1.438980.
[43] R. Krishnan, J. S. Binkley, R. Seeger, J. A. Pople, *J. Chem. Phys.* **1980**, *72*, 650. https://doi.org/10.1063/1.438955.
[44] C. J. Cramer, D. G. Truhlar, *Acc. Chem. Res.* **2008**, *41*, 760. https://doi.org/10.1021/ar800019z.
[45] F. M. Bickelhaupt, K. N. Houk, *Angew. Chem., Int. Ed.* **2017**, *56*, 10070. https://doi.org/10.1002/anie.201701486.
[46] P. Vermeeren, S. C. C. van der Lubbe, C. Fonseca Guerra, F. M. Bickelhaupt, T. A. Hamlin, *Nat. Protoc.* **2020**, *15*, 649. https://doi.org/10.1038/s41596-019-0265-0.
[47] F. M. Bickelhaupt, *J. Comput. Chem.* **1999**, *20*, 114. https://doi.org/10.1002/(SICI)1096-987X(19990115)20:1(114::AID-JCC12)3.0.CO;2-L.
[48] G. te Velde, F. M. Bickelhaupt, E. J. Baerends, C. Fonseca Guerra, S. J. A. van Gisbergen, J. G. Snijders, T. Ziegler, *J. Comput. Chem.* **2001**, *22*, 931.
[49] L. Zhao, M. von Hopffgarten, D. M. Andrada, G. Frenking, *WIREs Computational Molecular Science* **2018**, *8*, e1345. https://doi.org/10.1002/wcms.1345.
[50] F. M. Bickelhaupt, E. J. Baerends, in *Reviews in Computational Chemistry* **2000**, pp. 1.
[51] C. Hansch, A. Leo, R. W. Taft, *Chem. Rev.* **1991**, *91*, 165. https://doi.org/10.1021/cr00002a004.
[52] M. A. van Bochove, M. Swart, F. M. Bickelhaupt, *J. Am. Chem. Soc.* **2006**, *128*, 10738.
[53] A. T. P. Carvalho, M. Swart, J. N. P. van Stralen, P. A. Fernandes, M. J. Ramos, F. M. Bickelhaupt, *J. Phys. Chem. B* **2008**, *112*, 2511. https://doi.org/10.1021/jp7104665.
[54] T. A. Hamlin, M. Swart, F. M. Bickelhaupt, *ChemPhysChem* **2018**, *19*, 1315. https://doi.org/10.1002/cphc.201701363.
[55] M. A. van Bochove, M. Swart, F. M. Bickelhaupt, *ChemPhysChem* **2007**, *8*, 2452.
[56] A. P. Bento, F. M. Bickelhaupt, *J. Org. Chem.* **2008**, *73*, 7290. https://doi.org/10.1021/jo801215z.
[57] A. P. Bento, F. M. Bickelhaupt, *Chem Asian J* **2008**, *3*, 1783. https://doi.org/10.1002/asia.200800065.
[58] T. A. Hamlin, P. Vermeeren, C. Fonseca Guerra, F. M. Bickelhaupt in, (Eds: S. Grabowsky, De Gruyter), **2021**, pp. 199–212.

Manuscript received: August 27, 2025
Version of record online: October 9, 2025